

# Mapping Coupled Time-series Onto Complex Network

Jamshid Ardalankia<sup>a,b</sup>, Jafar Askari<sup>c</sup>, Somaye Sheykhali<sup>d,e</sup>, Emmanuel Haven<sup>f</sup>, G.Reza Jafari<sup>b,c,g</sup>

<sup>a</sup>Department of Financial Management, Shahid Beheshti University, G.C., Evin, Tehran, 19839, Iran

<sup>b</sup>Center for Complex Networks and Social Data Science, Department of Physics, Shahid Beheshti University, G.C., Evin, Tehran, 19839, Iran

<sup>c</sup>Department of Physics, Shahid Beheshti University, G.C., Evin, Tehran, 19839, Iran

<sup>d</sup>Department of Physics, University of Zanjan (ZNU), Zanjan, 45371-38791, Iran

<sup>e</sup>Instituto de Física Interdisciplinaria Sistemas Complejos IFISC (CSIC-UIB), Palma de Mallorca, E07122, Spain

<sup>f</sup>Faculty of Business Administration, Memorial University, St. John's, Canada and IQSCS, UK

<sup>g</sup>Department of Network and Data Science, Central European University, 1051 Budapest, Hungary

## Abstract

In order to extract hidden joint information from two possibly uncorrelated time-series, we explored the measures of network science. Alongside common methods in time-series analysis of the economic markets, mapping the joint structure of two time-series onto a network provides insight into hidden aspects embedded in the couplings. We discretize the amplitude of two time-series and investigate relative simultaneous locations of those amplitudes. Each segment of a discretized amplitude is considered as a node. The simultaneity of the amplitudes of the two time-series is considered as the edges in the network. The frequency of occurrences forms the weighted edges. In order to extract information, we need to measure that to what extent the coupling deviates from the coupling of two uncoupled series. Also, we need to measure that to what extent the couplings inherit their characteristics from a Gaussian distribution or a non-Gaussian distribution. We mapped the network from two surrogate time-series. The results show that the couplings of markets possess some features which diverge from the same features of the network mapped from white noise, and from the network mapped from two surrogate time-series. These deviations prove that there exist joint information and cross-correlation therein. By applying the network's topological and statistical measures and the deformation ratio in the joint probability distribution, we distinguished basic structures of cross-correlation and coupling of cross-markets. It was discovered that even two possibly known uncorrelated markets may possess some joint patterns with each other. Thereby, those markets should be examined as coupled and *weakly* coupled markets.

**Keywords:** Coupled Time-series, Complex Networks, Financial Markets

## 1. Introduction

It is intriguing to study the joint information of two time-series by mapping their coupling onto a network. Several added advantages appear if one investigates the two time-series after applying the surrogate method, and to then find the joint structures of those two time-series by mapping them onto a network. By this approach, the sources of coupled structures are revealed (correlation and fat-tailed distribution). The reasoning behind applying this procedure provides from the numerous measures in network science [1–4]. In order to extract more hidden information from time series, network science has been successfully utilized for analyzing the extracted information from time series coming from a wide variety of fields, all through the analysis of the derived network [5–12].

We investigate the coupling and cross-correlation of three financial time-series, DJIA, S&P500 and SSEC. As mentioned in [5], stock markets can be characterized as systems with joint structures and simultaneous behaviors and they can be analyzed by mapping their joint structures onto a network. Zhang *et al* [5]

introduced ordered patterns for some chaotic time-series. They mapped the evolution of patterns onto a network. This transition network formed a chain with forbidden patterns. The weighted edges correspond to the frequency of patterns. It was shown that by changing the parameters of the system dynamics in ordinal transition networks, the temporal evolution and forbidden phases in the network may change. Also, by mapping the trajectories and lagged effects of a dynamical system onto a network, one can form a Markov chain [13]. Some other methods have been applied to map time-series analysis to network science. For instance, visibility graphs [8, 14–17] reveal the structural topology of networks of coupled time-series in whether the time-series are random, periodic (ordered) or fractal. This will cause the mapping algorithm to result in respectively, a random network, regular network and scale-free network [8]. Mapping time-series onto a network is also employed by a visibility graph algorithm to assess network topological and statistical measures of financial markets with different Hurst exponents [16]. Mapping multi-variate time-series also result in multi-layer networks [18, 19]. The visibility graph method for mapping time-series onto a multi-layer network, has a wide applicability in machine learning [17]. A multi-scale mapping of time-series onto a network and the transmission of

Email addresses: ehaven@mun.ca (Emmanuel Haven),  
gjafari@gmail.com (G.Reza Jafari)

ordinal regression patterns between two time-series in the local trends of non-stationary time-series, provide for useful results too [20]. With respect to the cross-correlation networks [21], the network properties such as the clustering coefficient, the efficiency, the cross-correlation degree of cross-correlation interval and also the modularity of dynamic states, have all been investigated [22]. An example of another real-world application provides from the mapping of time-series onto a network in tourism management [23].

One of the main strengths of network science in dynamic systems can be found in higher-order analysis [24, 25]. Network analysis is of tremendous use in finance and economics. It helps scholars to explore deeper systemic risk evaluations [26–31]. We will compare the patterns in mapped networks of two market based time-series with the patterns in mapped networks with fractional Gaussian noises (fGns). FGns are known as specific random series with the range of anti-persistent, white noise, and persistent behavior where the so called Hurst exponent has relevance. The Hurst exponent is a criterion which informs to what extent two time-series are coupled in various time-scales [32–34]. The pattern of some measurements in network science shows that there is coupled information embedded in the joint systems. Some measurements are significantly close to the networks mapped from fGns. However, there exist measurements where none of the networks converge to a definite value. Based on the segregation of those networks, the information transitions and measurements with closer values are revealed. The coupling and cross-correlation in financial time-series intrinsically contain scaling behaviors [32–34]. Those scaling behaviours not only emerge in temporal aspects, but they also appear in higher statistical moments of price return distributions. In this context, the present study casts light into the behavior of the couplings between financial time-series by applying novel measures of network science.

We are supposed to capture temporal/dynamic behaviors of the financial time-series by mapping onto a network as follows, by:

- I. introducing the mapping algorithm from coupled time-series onto a network;
- II. constructing a network obtained by mapping the coupling of two financial time-series, and;
- III. constructing the networks mapped from fractional Gaussian noises (fGns) which are coupled by their 1-step lag with a range of Hurst exponents;
- IV. comparing the obtained networks and extracting the hidden features of couplings.

## 2. The Mapping Algorithm

As shown in Fig. 1, for two time-series:  $X(t) = \{x(t_1), x(t_2), \dots, x(t_N)\}$  and,  $Y(t) = \{y(t_1), y(t_2), \dots, y(t_N)\}$ , we have:

I- The joint probability matrix is constructed from these time-series. It will be the adjacency matrix of the network. The frequency of the above-mentioned conditions represents the weighted adjacency matrix among the two time-series.

II- The iteration occurs on the data-points  $t = 1, 2, \dots, N$ . The amplitudes of  $x(t)$  and  $y(t)$  are discretized to an equal number

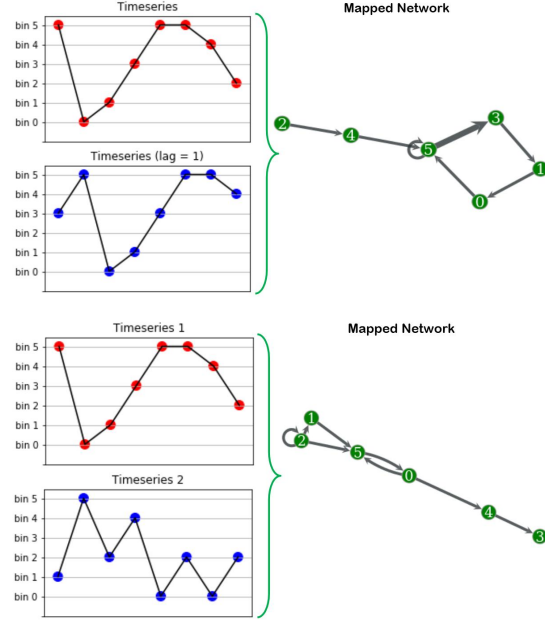


Figure 1: We demonstrate the mapping algorithm. This figure depicts the way links in the network are generated. As shown, when the amplitudes corresponding to two time-series are located in the same amplitude-bins (nodes), a weighted *self-loop* is considered. However, when the amplitudes are not located in the same bin, two nodes connecting with a weighted *edge* are generated. The term *weight* implies the frequency of this directed situation– and can be applied with the persistence of edges [35]. The outcome will be a temporal network.

of bins, and each bin is considered as a node in the network.

III- For any  $t = t_n$ :

If  $x(t_n) = y(t_n) = i$ : a self-loop for the node (bin)  $i$  is constructed.

If  $x(t_n) = i$  and,  $y(t_n) = j, i \neq j$ : an edge between nodes  $i$  and  $j$  is constructed.

The number of bins is a matter of trade-off. A high number of bins shortens the width of bins. Hence, extremely narrow bins contribute to noise detection. Conversely, extremely wide bins contribute to extremely low information extraction. Considering the amplitude-wise scaling features of financial correlations [32–34], alongside the fact that the correlation coefficients just reveal linear co-behaviors, there exists a vital need to consider the effects of direction and size of the fluctuations. Those amplitudes may contain nonlinear behaviors. Hence, in our work without the need for necessarily linear relations, the couplings are defined. This procedure can be explored by both temporal-intervals [22] and amplitude-intervals [9]. We generate discrete intervals to evaluate the amplitude of the markets and we then map those amplitudes (nodes) and their relations (edges) onto a network.

## 3. Mapping Single Time-series Onto a Network

We discretize the amplitudes of a series and also its 1-step-lag series. By this segmentation and by converting them onto several bins [9], we couple those amplitudes. We consider these amplitude-bins as nodes in a network. The top subfigure in

Fig. 1, shows the way we design the algorithm. The Hurst exponent of a system implies how two time-series –also one single time-series and its lags– have a coupling in a persistent (Hurst>0.5), white noise (Hurst=0.5), and anti-persistent (Hurst<0.5) manner. This is an intrinsic and a structural characteristic of developed and emerging financial markets [32]. Initially, we generate a total of 288 fractional Gaussian noises (fGns) with Hurst exponents ranging from anti-persistence to persistence (0.1 to 0.9) and 2000 data-points for each series. A high Hurst exponent is an identification of stronger coupling. Respecting the shape of joints and their resulting networks, in Fig. 2, it is depicted that a high Hurst exponent leads to a high elongation around the main diameter of joint probabilities. To quantify the elongation of couplings, we introduce a deformation parameter,  $R$ , based on the standard deviations along diameters of joint probabilities. This parameter widely clarifies the couplings behavior, and it is quantified by Eq. 1;

$$R = \frac{\sigma_i - \sigma_j}{\max\{\sigma_i, \sigma_j\}}; \quad (1)$$

where,  $\sigma$  denotes the standard deviations along the diameters of the joint probability matrix. The relationship between the parameter  $R$  relative to the corresponding Hurst exponents is shown in Fig. 2.

#### 4. Mapping Coupled Time-series Onto a Network

We map the coupling of two market time-series onto a network. The algorithm which is applied here, is the same as the previous one. However, two time-series with the simultaneous chronological time-stamp (no lag) are considered. The outcome will be compared with the fGns which are already mapped onto the network (Fig. 3). In Fig. 1, in addition to considering the positive and negative amplitudes, we account for the differences between the amplitudes. The placement of amplitudes in the same amplitude-bin, leads to a self-loop. On the other hand, the placement of amplitudes in different amplitude-bins leads to an edge. The direction of edges stands for emphasizing the difference between whether the first signal is in bin A and the other one in B, as opposed to whether the first signal is in bin B and the second one in A.

#### 5. Results and Discussion

In Fig. 3, radar plots a) and b), 20 topological and statistical measurements of the obtained networks from the cross-markets are compared with those from fGns and those from surrogate time-series. It is notable that a fGn with Hurst=0.5 is the indication of no coupling. The convergence of any cross-market measurement to the measurement related to Hurst=0.5, illustrates insignificant information embedded in the coupling. Despite the segregation among the measurements of different joint systems, there exist some similarities. As shown in Fig. 3, the DJIA-SSEC's coupling is closer to an uncoupled situation rather than DJIA-S&P500's coupling. In radar plot b), the same measurements are reported for the joints of surrogate

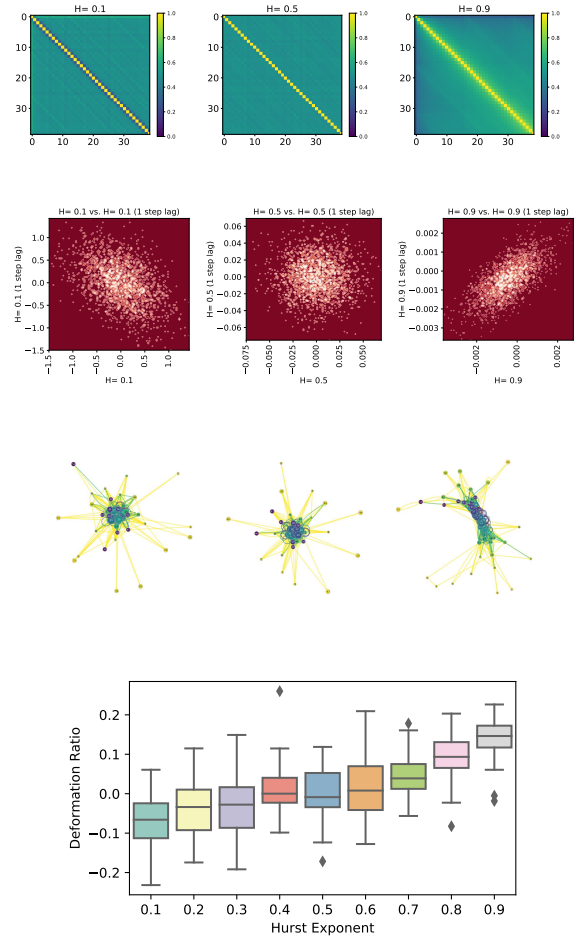


Figure 2: The general temporal pattern of an anti-persistent (Hurst<0.5), white noise (Hurst=0.5) and persistent (Hurst>0.5) systems are demonstrated; 1st row) The auto-correlation matrices relating to Hurst= 0.1, 0.5, 0.9; 2nd row) Adjacency Matrices relating to Hurst= 0.1, 0.5, 0.9; 3rd row) The Network's Topology of time-series with Hurst= 0.1, 0.5, 0.9; 4th row) Deformation ratio  $R$  versus their corresponding Hurst exponents are shown. As shown, the general trend of the deformation ratio (in Eq. 1) versus the Hurst exponent is ascending.

DJIA vs. surrogate SSEC, and also, for the joints of surrogate DJIA vs. surrogate S&P500. A non-Gaussian time-series gives up its non-Gaussianity by surrogate method. Hence, it does not have any effect on the fGns. The sources of different coupling between time-series stem from two phenomena: correlation, and fat-tailed distribution. After surrogate method, the correlation remains, but the probability distribution converts to a Gaussian distribution. To consider more extensive test systems, in radar plot b), the market series are surrogated (see Appendix A) and the coupling of surrogate series were mapped to a network. The outcome is interesting where the patterns have higher conformity rather than the original time-series in radar plot a). Radar plot b) shows that, after surrogate method, the deviations which their sources relate to the fat-tailed PDFs, come closer to each other. It means that the deviations with the source of non-Gaussianity are eliminated, and the deviations with merely the source of correlation remain.

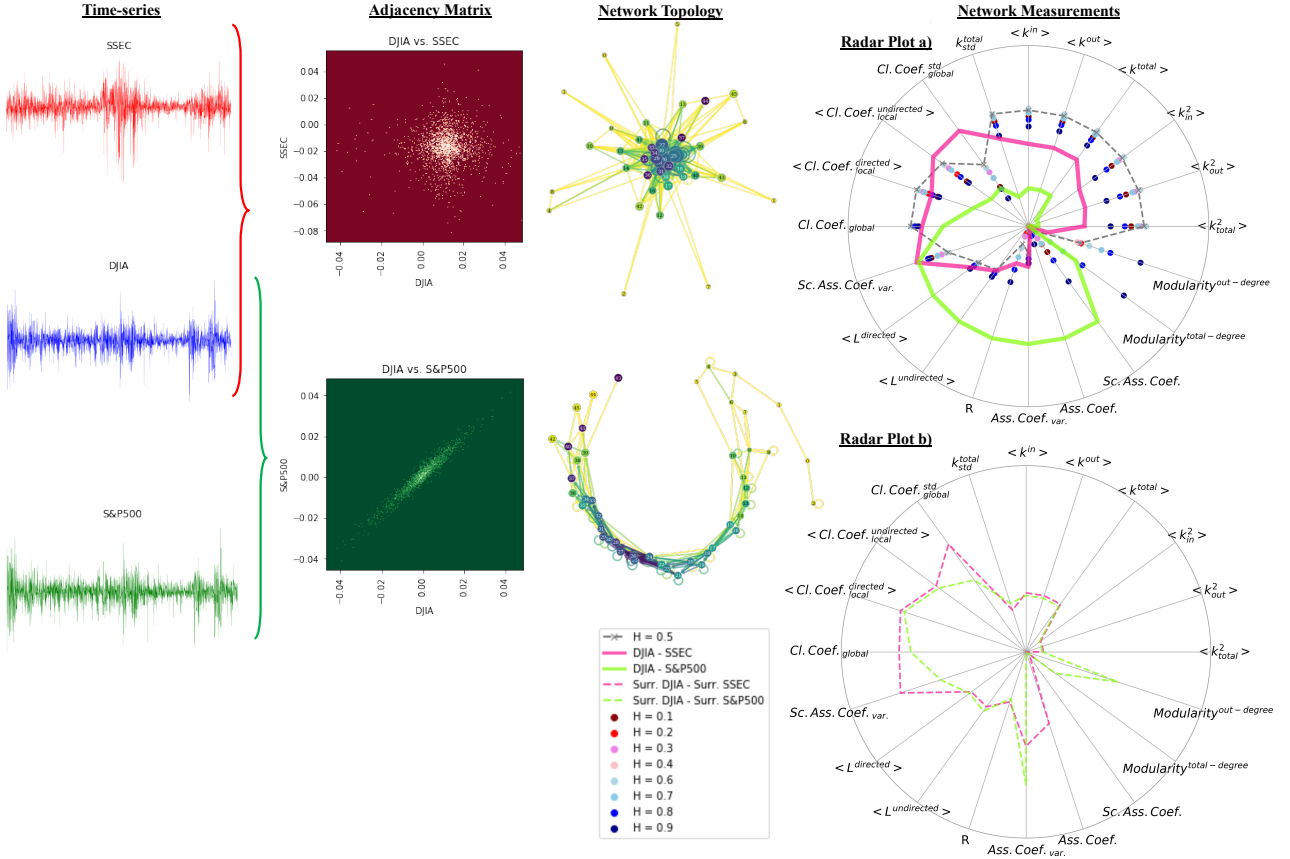


Figure 3: The mapping of the coupling of time-series onto a network is shown: from left, the 1st column shows the time-series of the markets such as SSEC, DJIA and S&P500 in daily resolution during 2000 days until Jul. 31<sup>st</sup> 2019; the 2nd column depicts DJIA-SSEC adjacency matrix and DJIA-S&P500 adjacency matrix; the 3rd column illustrates the topology of networks corresponding to DJIA-SSEC coupling and DJIA-S&P500 coupling—simulated by Graph-tool [36]. The radar plots on the right side provide fully comparative topological and statistical features of the networks. Radar plot (a) shows significant deviating patterns between networks mapped from joint series. Since the obtained networks are significantly different from each other, it proves that the type of couplings are typically different. To consider more extensive test systems, in radar plot (b), the market series are surrogated (see Appendix A) and the coupling of surrogated series are mapped to the network. The outcome is interesting where the patterns are higher conformity rather than the original time-series in radar plot (a). Hence, radar plot (b) shows that, after surrogate method, the deviations which their sources relate to the fat-tailed PDFs, come closer to each other. This means that the deviations, with the source of non-Gaussianity, are eliminated and the deviations with merely the source of correlation remain.

- *Deformation Ratio (R)*: In Fig. 3 a comparison between joint probability matrices of DJIA-SSEC and DJIA-S&P500 is shown. The strength of couplings are visually shown. The coupling of DJIA-S&P500 is stronger than that of DJIA-SSEC. This feature is quantified based on Eq. 1 with the  $R$  parameter which is considered in the radar plots in Fig. 3.

- *Degree Measurements*: The measurements corresponding to degrees, such as mean squared out-degrees  $\langle k_{out}^2 \rangle$ , mean squared in-degrees  $\langle k_{in}^2 \rangle$ , mean squared total-degrees  $\langle k_{total}^2 \rangle$ , mean out-degrees  $\langle k_{out} \rangle$ , mean in-degrees  $\langle k_{in} \rangle$  and mean total-degrees  $\langle k_{total} \rangle$ , contain significant power for proving the segregation among cross-markets and the fGn with Hurst=0.5. The mentioned features in the radar plots in Fig 3 contain significant coupling information among fGns and also the cross-market coupling mapped onto a network. Also, the standard deviation of total-degree  $\langle k_{std}^{total} \rangle$  turns up to identify cross-market couplings.

- *Clustering Measurements [37]*: The standard deviation of

the global clustering coefficient  $Cl.Coeff_{global}^{std}$  is capable of exploring the difference between cross-market couplings. The undirected local clustering coefficient  $Cl.Coeff_{local}^{undirected}$  can distinguish among the networks of coupled and uncoupled cross-markets. This feature converges to a fGn with Hurst=0.5 for the network extracted from an uncoupled cross-market. Also, the directed local clustering coefficient  $Cl.Coeff_{local}^{directed}$  is different for uncoupled and coupled outcomes. The global clustering coefficient  $Cl.Coeff_{global}$  for fGns, uncoupled and coupled cross-markets are approximately similar.

- *Length (Shortest Path Between Pair-wise Vertices) Measurements*: It is striking that the directed mean length  $\langle L^{directed} \rangle$  and the undirected mean length  $\langle L^{undirected} \rangle$  significantly explore the differences between coupled cross-markets from uncoupled cross-markets and the fGns.

- *Assortativity Measurements [2]*: The variance of scalar assortativity coefficient  $Sc.Ass.Coeff_{var.}$  for fGns, uncoupled and coupled cross-markets are approximately similar. Con-

Couplings	$\langle k^2_{total} \rangle$	$\langle k^2_{out} \rangle$	$\langle k^2_{in} \rangle$	$\langle k^{total} \rangle$	$\langle k^{out} \rangle$	$\langle k^{in} \rangle$	$\langle k^{total}_{sd} \rangle$	$Cl.Coeff_{global}^{sd}$	$\langle Cl.Coeff_{local}^{undirected} \rangle$	$\langle Cl.Coeff_{local}^{directed} \rangle$
fGn(H=0.3)	1539.4886+/-78.7488	385.9506+/-19.7517	386.1561+/-19.7614	30.5858+/-1.525	15.2929+/-0.7625	15.2929+/-0.7625	3.0424+/-0.15	0.0194+/-0.001	0.8481+/-0.0422	0.5165+/-0.0258
fGn(H=0.5)	1595.5203+/-80.9523	400.1648+/-20.3541	400.1184+/-20.2721	31.125+/-1.5474	15.5625+/-0.7737	15.5625+/-0.7737	3.1006+/-0.1527	0.0221+/-0.0011	0.9208+/-0.0454	0.5478+/-0.0272
fGn(H=0.7)	1507.9394+/-77.9357	378.3426+/-19.6152	378.1347+/-19.5056	30.4147+/-1.5221	15.2073+/-0.761	15.2073+/-0.761	2.9856+/-0.147	0.0173+/-0.0009	0.8205+/-0.0408	0.508+/-0.0251
DJIA-SSEC	794.5777	212.0666	223.2222	22.7111	11.3555	11.3555	2.4890	0.0351	1.0437	0.4873
DJIA-S&P500	140.5777	37.1777	34.8666	10.4444	5.2222	5.2222	0.8365	0.0140	0.4092	0.2770

Couplings	$Cl.Coeff_{global}$	$Sc.Ass.Coeff_{var}$	$\langle L^{directed} \rangle$	$\langle L^{undirected} \rangle$	$R$ from Eq. 1	$Ass.Coeff_{var}$	$Ass.Coeff.$	$Sc.Ass.Coeff.$	$modularity^{total-degree}$	$modularity^{out-degree}$
fGn(H=0.3)	0.6983+/-0.0343	0.0316+/-0.0016	1.7528+/-0.0862	1.565+/-0.077	-0.0258+/-0.0234	0.0066+/-0.0003	-0.0049+/-0.0008	-0.0799+/-0.0079	-0.0025+/-0.0016	-0.0024+/-0.002
fGn(H=0.5)	0.7011+/-0.0345	0.0292+/-0.0014	1.7269+/-0.0848	1.5484+/-0.076	0.0006+/-0.02	0.0066+/-0.0004	-0.0035+/-0.0007	-0.1358+/-0.0117	-0.0024+/-0.0014	-0.0016+/-0.0018
fGn(H=0.7)	0.688+/-0.0339	0.0331+/-0.0016	1.7813+/-0.0874	1.5886+/-0.0779	0.0468+/-0.0163	0.0072+/-0.0004	0.0008+/-0.0009	-0.0338+/-0.0087	0.0072+/-0.0015	0.0095+/-0.0019
DJIA-SSEC	0.6523	0.0419	2.0138	1.6237	0.0690	0.0102	0.0006	-0.1917	-0.0052	-0.0197
DJIA-S&P500	0.5221	0.0411	3.3819	3.4666	0.3414	0.0297	0.1491	0.6630	0.0118	-0.0304

Table 1: To test the reliability and robustness of the results, we estimated the mean interval of each measurement for the network obtained from fGns. The estimated interval for each measurement is calculated with the confidence level of 90% by  $\bar{x} - Z_{(1-\frac{\alpha}{2})=0.95} \times \frac{S}{\sqrt{n}} < \mu < \bar{x} + Z_{(1-\frac{\alpha}{2})=0.95} \times \frac{S}{\sqrt{n}}$ ; where  $\mu$  is the measurement value.  $\bar{x}$ ,  $S$  and  $n$  stand for the sample mean, the sample standard deviation and the number of generated samples, respectively. As shown, the results in the table conform with Fig. 3. Some measurements in the DJIA-SSEC mapped network and the DJIA-S&P500 mapped network have similarity with the measurements generated by fGns and some have larger deviations.

versely, the assortativity coefficient variance  $Ass.Coeff_{var}$ , assortativity coefficient  $Ass.Coeff.$ , scalar assortativity coefficient  $Sc.Ass.Coeff.$  markedly distinguish among coupled cross-markets from fGns and uncoupled cross-markets.

- *Modularity Measurements* [3, 4]: As shown in Fig. 3 notwithstanding that out-degree modularity enables one to identify the cross-markets from fGn, the total-degree modularity  $Modularity^{total-degree}$  is highly capable of showing the divergence between uncoupled and coupled cross-markets. Based on the out-degree modularity measurement, there exists mutual information among markets and it is not uncoupled in this manner. In this regard, markets are coupled or weakly coupled (not necessarily uncoupled).

To further assess the patterns, DJIA-S&P500's coupling is adequately far from white noise (a fGn with Hurst = 0.5) and DJIA-SSEC's coupling. The flipside of the coin is that DJIA-SSEC's coupling is closer to white noise (an fGn with Hurst = 0.5) rather than DJIA-S&P500, but it is still totally different. Although the joint probabilities of DJIA and SSEC's time-series show that they are uncoupled (Eq. 1 and Fig. 3), by mapping the coupling of two time-series onto a network, more hidden properties are revealed. According to some other network measurements, those markets still possess coupling information. Hence, being a market contributes to being coupled with others. Thus, it is better to use the term, *weakly coupled markets* rather than the term, *uncoupled markets*. Along with giving us the ability to measure the coupling constituents between two time-series, Fig. 3 will extend our knowledge toward realistic simulations in joint structures within a network perspective.

Financial shocks contribute to contagion through alteration in couplings and dependencies [38]. Our results by mapping the couplings [32, 33] onto a network have applications in diverse risk measurement approaches with internal and multilateral interactions in economic and financial networks [26, 27], and crisis analysis [28–31]. If an economist can distinguish where the sources of couplings stem from, and under what circumstances the prices change simultaneously, they can find out how to conform an investment portfolio so to lower the risk. It is of great importance to know how couplings are formed from the PDFs and their tails. To explain it more in details we have:

- *Degree Measurements*: The tails of the PDF possess lower degrees, and, the nodes near the mean value possess higher degrees.  $\langle k >^2$  contains more information about the tails as opposed to  $\langle k^2 \rangle$ . Conversely,  $\langle k^2 \rangle$  contains more information about the mean value as opposed to  $\langle k >^2$ . Hence, the relation  $\frac{\langle k >^2}{\langle k^2 \rangle}$  contains vital information about the source of coupling, i.e. whether the coupling stems from a fat tail distribution or the Gaussian distribution. High  $\frac{\langle k >^2}{\langle k^2 \rangle}$  means that tails contain a higher share in the couplings. Low  $\frac{\langle k >^2}{\langle k^2 \rangle}$  implies that the tails contain a smaller share in the couplings.

- *Assortativity*: A high assortativity means that a high-degree component usually create links with the high-degree ones, and vice versa. It implies the system tends to preserve its trend. The disassortativity quantity implies that a big jump tends to a small movement.

- *Modularity*: Each node is a price return. Modularity shows that the changes within a community are more probable than between two communities. It can be assessed whether the modularity is a mathematical language for the terms ‘‘support’’ and ‘‘resistance’’ in technical market analysis. High modularity implies that the corresponding price returns of the two markets follow simultaneous similar changes.

- *Mean Length*: It declares that on average how agents (say amplitudes in our case) can create a relation with each other. In other words, it shows to what extent the system can translate its dynamic.

- *Deformation Ratio*: It is applied to quantify the joint probability shape. Based on the deformation ratio, one can find out how two joint-markets are extended in comparison with an uncoupled market.

- *Clustering Coefficient*: A high clustering coefficient states the extent to which the agents in the system tend to remain in their clusters. In our case, the amplitudes resist to change their clusters.

Even two previously known uncoupled and uncorrelated markets may possess coupled characteristics. Hence, those markets should be examined as coupled and *weakly* coupled markets.

## 6. Conclusion

Mapping the cross-correlation of two coupled time-series onto a network helps scholars to gain more insight into the im-

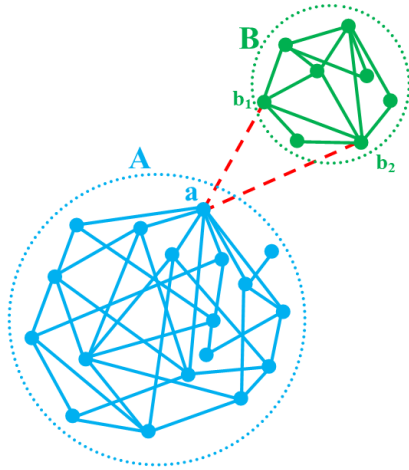


Figure 4: This figure schematically shows two communities (A and B). There are certain nodes (price returns) that can connect both communities via those nodes (price returns)  $-a$  to  $b_1$  and  $b_2$  (via red dashed lines). Inter-community movements from one node (price return) to another node (another price return) is more probable, and intra-community movements are less probable. Thereby, higher modularity leads to lower homogeneity in the likelihood of movements throughout the whole network. Indeed, modularity quantifies the heterogeneity of the possibility of the inter-community and intra-community of movements.

portant constituents of joint structures between two time-series. Topological and statistical parameters along with the *deformation ratio of joint probability between two time-series* (which is extracted from the standard deviations along both diameters of the directed weighted adjacency matrix) are able to reveal the coupling information which has previously been beyond the reach of researchers. Comparing the network mapped from fGns and from joint markets structures, not only proves pairwise inter-connectedness, it also clarifies the diverse structure of the coupling and cross-correlation therein. The reasoning behind this claim is that couplings with different Hurst exponents show a diverse range of behaviours (anti-persistent, white noise, persistent). Those behaviours can be reflected in a network from mapping the joint structures to that network. Also, the network mapped from joint structures of surrogate time-series in Fig. 3 proves that the coupling is derived from two criteria: cross-correlation, and a fat-tailed PDF.

## 7. Appendix A

The surrogate method converts the non-Gaussian PDF to the Gaussian PDF. Although surrogate method eliminates the non-linear structure in the time-series, it maintains the linear structure. The outcome gets closer to a Gaussian process. Through a Fourier surrogate, after the phase randomization process, the central limit theorem is satisfied. Given a time-series named  $X(t)$ , the discrete Fourier transform of  $X(t)$  is given by:

$$X(\omega) = \frac{1}{N} \sum_t X(t) \exp(i\omega t); \quad (2)$$

Then, the phase of the time-series is randomized by a pseudo-independent uniform distribution set,  $\eta$ . Thereby, we have:

$$X^*(\omega) = \sum_{\omega} |X(\omega)| \exp(-i\eta\omega); \quad (3)$$

Since sine and cosine values in Eq. 2 occur within  $[-1,1]$ ,  $X_{max}(\omega) \leq X_{max}(t)$ , and  $x(t) \neq \infty$ , then  $X(\omega)$  has finite mean and variance. Hence, based on the central limit theorem in a randomization procedure, the PDF translates to a Gaussian PDF. Accordingly, by applying a reverse discrete Fourier transform on  $X^*$ , the resulting phase randomized time-series is Gaussian [34].

## References

- [1] A.-L. Barabási, R. Albert, H. Jeong, Mean-field theory for scale-free random networks, *Physica A: Statistical Mechanics and its Applications* 272 (1-2) (1999) 173–187. doi:10.1016/s0378-4371(99)00291-5.
- [2] M. E. J. Newman, The structure and function of complex networks, *SIAM Review* 45 (2) (2003) 167–256. doi:10.1137/s003614450342480.
- [3] M. E. J. Newman, Modularity and community structure in networks, *Proceedings of the National Academy of Sciences* 103 (23) (2006) 8577–8582. doi:10.1073/pnas.0601602103.
- [4] M. E. J. Newman, M. Girvan, Finding and evaluating community structure in networks, *Physical Review E* 69 (2). doi:10.1103/physreve.69.026113.
- [5] J. Zhang, J. Zhou, M. Tang, H. Guo, M. Small, Y. Zou, Constructing ordinal partition transition networks from multivariate time series, *Scientific Reports* 7 (1). doi:10.1038/s41598-017-08245-x.
- [6] Y. Zou, R. V. Donner, N. Marwan, J. F. Donges, J. Kurths, Complex network approaches to nonlinear time series analysis, *Physics Reports* 787 (2019) 1–97. doi:10.1016/j.physrep.2018.10.005.
- [7] X. Sun, M. Small, Y. Zhao, X. Xue, Characterizing system dynamics with a weighted and directed network constructed from time series data, *Chaos: An Interdisciplinary Journal of Nonlinear Science* 24 (2) (2014) 024402. doi:10.1063/1.4868261.
- [8] L. Lacasa, B. Luque, F. Ballesteros, J. Luque, J. C. Nuno, From time series to complex networks: The visibility graph, *Proceedings of the National Academy of Sciences* 105 (13) (2008) 4972–4975.
- [9] A. H. Shirazi, G. R. Jafari, J. Davoudi, J. Peinke, M. R. R. Tabar, M. Sahimi, Mapping stochastic processes onto complex networks, *Journal of Statistical Mechanics: Theory and Experiment* 2009 (07) (2009) P07046. doi:10.1088/1742-5468/2009/07/p07046.
- [10] A. S. L. O. Campanharo, M. I. Sirer, R. D. Malmgren, F. M. Ramos, L. A. N. Amaral, Duality between time series and networks, *PLOS ONE* 6 (8) (2011) e23378. doi:10.1371/journal.pone.0023378.
- [11] Z. Zhang, J. Xu, X. Zhou, Mapping time series into complex networks based on equal probability division, *AIP Advances* 9 (1) (2019) 015017. doi:10.1063/1.5062590.
- [12] R. Jacob, K. P. Harikrishnan, R. Misra, G. Ambika, Weighted recurrence networks for the analysis of time-series data, *Proceedings of the Royal Society A: Mathematical, Physical and Engineering Sciences* 475 (2221) (2019) 20180256. doi:10.1098/rspa.2018.0256.
- [13] M. McCullough, M. Small, T. Stemler, H. H.-C. Iu, Time lagged ordinal partition networks for capturing dynamics of continuous dynamical systems, *Chaos: An Interdisciplinary Journal of Nonlinear Science* 25 (5) (2015) 053101. doi:10.1063/1.4919075.
- [14] H. Xiong, P. Shang, J. He, Nonuniversality of the horizontal visibility graph in inferring series periodicity, *Physica A: Statistical Mechanics and its Applications* 534 (2019) 122234. doi:10.1016/j.physa.2019.122234.
- [15] B. Luque, L. Lacasa, F. Ballesteros, J.-G. Luque, Horizontal visibility graphs: exact results for random time series., *Physical review. E, Statistical, nonlinear, and soft matter physics* 80 4 Pt 2 (2009) 046103.
- [16] M. Stephen, C. Gu, H. Yang, Visibility graph based time series analysis, *PLOS ONE* 10 (11) (2015) e0143015. doi:10.1371/journal.pone.0143015.

- [17] F. M. Bianchi, L. Livi, C. Alippi, R. Jenssen, Multiplex visibility graphs to investigate recurrent neural network dynamics, *Scientific Reports* 7 (1). doi:10.1038/srep44037.
- [18] L. Lacasa, V. Nicosia, V. Latora, Network structure of multivariate time series, *Scientific Reports* 5 (1). doi:10.1038/srep15508.
- [19] S. Boccaletti, G. Bianconi, R. Criado, C. I. Del Genio, J. Gómez-Gardenes, M. Romance, I. Sendina-Nadal, Z. Wang, M. Zanin, The structure and dynamics of multilayer networks, *Physics Reports* 544 (1) (2014) 1–122.
- [20] X. Gao, H. An, W. Fang, X. Huang, H. Li, W. Zhong, Y. Ding, Transmission of linear regression patterns between time series: From relationship in time series to complex networks, *Physical Review E* 90 (1). doi:10.1103/physreve.90.012818.
- [21] S. Mehraban, A. H. Shirazi, M. Zamani, G. R. Jafari, Coupling between time series: A network view, *EPL (Europhysics Letters)* 103 (5) (2013) 50011. doi:10.1209/0295-5075/103/50011.
- [22] C. Feng, B. He, Construction of complex networks from time series based on the cross correlation interval, *Open Physics* 15 (1) (2017) 253–260. doi:10.1515/phys-2017-0028.
- [23] R. Baggio, R. Sainaghi, Mapping time series into networks as a tool to assess the complex dynamics of tourism systems, *Tourism Management* 54 (2016) 23–33. doi:10.1016/j.tourman.2015.10.008.
- [24] Y. Zhang, A. Garas, I. Scholtes, Controllability of temporal networks: An analysis using higher-order networks, arXiv preprint arXiv:1701.06331.
- [25] R. Lambiotte, M. Rosvall, I. Scholtes, From networks to optimal higher-order models of complex systems, *Nature Physics* 15 (4) (2019) 313–320. doi:10.1038/s41567-019-0459-y.
- [26] S. Battiston, G. Caldarelli, M. D’Errico, *The Financial System as a Nexus of Interconnected Networks*, Springer International Publishing, Cham, 2016, pp. 195–229. doi:10.1007/978-3-319-23947-7\_12.
- [27] C. Perillo, S. Battiston, A multiplex financial network approach to policy evaluation: the case of euro area quantitative easing, *Applied Network Science* 3 (1) (2018) 49. doi:10.1007/s41109-018-0098-8.
- [28] H. Amini, R. Cont, A. Minca, Resilience to contagion in financial networks, *SSRN Electronic Journal* doi:10.2139/ssrn.1865997.
- [29] A. H. Shirazi, A. A. Saberi, A. Hosseiny, E. Amirzadeh, P. T. Simin, Non-criticality of interaction network over system’s crises: A percolation analysis, *Scientific Reports* 7 (1). doi:10.1038/s41598-017-16223-6.
- [30] R. Kaushik, S. Battiston, Credit default swaps drawup networks: Too interconnected to be stable?, *PLoS ONE* 8 (7) (2013) e61815. doi:10.1371/journal.pone.0061815.
- [31] J. Etesami, A. Habibnia, N. Kiyavash, Econometric modeling of systemic risk: going beyond pairwise comparison and allowing for nonlinearity.
- [32] J. Ardalankia, M. Osoolian, E. Haven, G. R. Jafari, Scaling features of price–volume cross correlation, *Physica A: Statistical Mechanics and its Applications* (2020) 124111 doi:10.1016/j.physa.2019.124111.
- [33] P. Caraiiani, E. Haven, Evidence of multifractality from CEE exchange rates against euro, *Physica A: Statistical Mechanics and its Applications* 419 (2015) 395–407. doi:10.1016/j.physa.2014.06.043.
- [34] L. Hedayatifar, M. Vahabi, G. R. Jafari, Coupling detrended fluctuation analysis for analyzing coupled nonstationary signals, *Physical Review E* 84 (2) (2011) 021138. doi:10.1103/physreve.84.021138.
- [35] L. E. C. Rocha, N. Masuda, P. Holme, Sampling of temporal networks: Methods and biases, *Physical Review E* 96 (2017) 052302. doi:10.1103/PhysRevE.96.052302.
- [36] T. P. Peixoto, The graph-tool python library, figshare doi:10.6084/m9.figshare.1164194.
- [37] D. J. Watts, S. H. Strogatz, Collective dynamics of ‘small-world’ networks, *Nature* 393 (6684) (1998) 440–442. doi:10.1038/30918.
- [38] I. Medovikov, A. Prokhorov, A new measure of vector dependence, with applications to financial risk and contagion, *Journal of Financial Econometrics* 15 (3) (2017) 474–503. doi:10.1093/jjfinec/nbx015.